ADVANCES IN ATMOSPHERIC SCIENCES, VOL. 39, FEBRUARY 2022, 333–343

• **Original Paper** •

A Climatological Perspective on Extratropical Synoptic-Scale Transient Eddy Activity Response to Western Pacific Tropical Cyclones※

Yao HA[1,2], Zhong ZHONG[*1,2,3], Haikun ZHAO[3], Yimin ZHU[1,2], Yao YAO[1], and Yijia HU[1]

[1]*College of Meteorology and Oceanography*, *National University of Defense Technology*, *Changsha* 410073, *China*

[2]*Jiangsu Collaborative Innovation Center for Climate Change and School of Atmospheric Sciences*, *Nanjing University*, *Nanjing* 210023, *China*

[3]*Key Laboratory of Meteorological Disaster of Ministry of Education*, *and Collaborative Innovation Center on Forecast and Evaluation of Meteorological Disasters*, *Nanjing University of Information Sciences and Technology*, *Nanjing* 210044, *China*

(Received 4 November 2020; revised 11 November 2021; accepted 23 November 2021)

ABSTRACT

An observational study focusing on the contribution of tropical cyclones (TCs) that form over the western North Pacific (WNP) to the synoptic-scale transient eddy activity (STEA) over the North Pacific during the boreal autumn and early winter in the period 1979–2019 is presented in this paper. Statistical results show that WNP TCs entering the mid-latitudinal North Pacific provide significant positive effects on the pentad mean strength of STEA, which is primarily concentrated over the Kuroshio/Oyashio Extensions (KOE) and regions from east of Japan to 160°W in the lower and mid-to-upper troposphere, respectively. TC intensity is highly indicative of the subsequent STEA with a correlation coefficient of 0.37/0.33/0.45 at 300 hPa/500 hPa/850 hPa exceeding the 99% confidence level for the period 1979–2019. The strength of STEA in the upper troposphere associated with TCs presents a more significant linear growth with TC intensity than that at the mid-to-lower levels after the cyclones enter the KOE region, suggesting that the impact of TCs on STEA gradually increases with height. Further analyses reveal that the contribution of TCs accounts for 4%–6% of the total STEA change over the KOE region during the late autumn and early winter. In addition, the influence of TCs on STEA experienced an interdecadal decrease from the early 2000s through the early 2010s.

Key words: Synoptic-scale transient eddy activity, tropical cyclone, North Pacific, Kuroshio/Oyashio Extensions, mid-latitudinal atmospheric motion

Citation: Ha, Y., Z. Zhong, H. K. Zhao, Y. M. Zhu, Y. Yao, and Y. J. Hu, 2022: A climatological perspective on extratropical synoptic-scale transient eddy activity response to western Pacific tropical cyclones. *Adv. Atmos. Sci.*, **39**(2), 333–343, https://doi.org/10.1007/s00376-021-0375-9.

Article Highlights:

- Tropical cyclone intensity is highly indicative of subsequent synoptic-scale transient eddy activity for the period 1979–2019.
- Tropical cyclones' impact on the strength of synoptic-scale transient eddy activity gradually increases with height.
- The contribution of tropical cyclones to synoptic-scale transient eddy accounts for 4%–6% of its total change from October to December.

1. Introduction

One of the strongest atmospheric baroclinic motions globally is located over midlatitude East Asia and the North Pacific and is characterized by vigorous synoptic-scale transient eddy activity (STEA; Ren et al., 2010, 2011; Xiao and Zhang, 2015). Daily weather changes in the midlatitudes are closely related to these active synoptic-scale systems transporting atmospheric energy from the subtropics to higher latitudes, which can dramatically affect the climate system as a whole (Chang et al., 2002). STEA exhibits complex changes in temporal variability over the mid-latitudinal North Pacific (Chang, 2001). During the annual cycle, there

※ This paper is a contribution to the special issue on Climate Change and Variability of Tropical Cyclone Activity.

* Corresponding author: Zhong ZHONG
Email: zhong_zhong@yeah.net

is a minimum in the strength of the climatological STEA over the North Pacific in midwinter (Nakamura, 1992). Before and after midwinter, the STEA reaches its two strongest intensity peaks during autumn to early winter (October to December) and the subsequent spring (March and April), respectively. This phenomenon is possibly related to the changes of upstream seed-like disturbances (Orlanski, 2005; Chang and Guo, 2007; Penny et al., 2010), the winter subtropical jet stream (Nakamura and Sampe, 2002; Chen et al., 2017), and oceanic diabatic heating (Chang and Song, 2006). On the other hand, the tropical cyclones (TCs) that form over the western North Pacific (WNP) monsoon trough are still active from autumn to early winter (Chan, 2000; Chia and Ropelewski, 2002; Wang and Chan, 2002; Ha et al., 2013; Zhao and Wang, 2016), and they transport plentiful momentum and moisture to the mid-to-higher latitudes while moving poleward (Harr and Dea, 2009; Cordeira et al., 2013; Keller, 2017). Meanwhile, some northeastward-moving intense TCs are transformed into extratropical cyclones with the structure of baroclinic low-pressure vortices when they move into the Kuroshio/Oyashio Extensions (KOE) region (Harr et al., 2000; Archambault et al., 2013; Grams and Archambault, 2016). TCs may supply downstream impacts on the midlatitude flow via the Rossby wave dispersion from the TC interacting with the extratropical waveguide and wave-mean flow interaction (Keller et al., 2019).

Based on the overlapping active periods and the consistency in terms of spatiotemporal variations between STEA and TC activity from October to December, the following scientific questions are addressed in this study using observational analyses: (1) STEA intensity in the midlatitude Pacific reaches its peaks in late autumn and early winter when TC activity in the western Pacific is still active; is STEA intensity sensitive to changes in TC activity? (2) Including extratropical and tropical cyclones, what is the general contribution of all cyclones to STEA changes over the KOE region? The purpose of this study is to reveal the potential contribution from TC activity to STEA intensity during autumn and early winter from a climatological perspective. This paper is organized as follows: The data and methods used in this study are described in section 2. The relationship between TC intensity and STEA over the KOE region during 1979–2019 is presented in section 3.1. The interannual variation of the contribution of TCs to STEA is analyzed in section 3.2. Finally, sections 4 and 5 present discussions and concluding remarks, respectively.

2. Data and methods

The reanalysis datasets used in this study include the horizontal velocity fields with spatial resolution of 2.5° × 2.5° at 17 pressure levels and at 6-hour intervals, extracted from the National Centers for Environmental Prediction-National Center for Atmospheric Research Reanalysis Project Dataset (NNRP; Kalnay et al., 1996; http://www.esrl.noaa.gov/psd/data/gridded/data.ncep.reanalysis.html). We also use TC best-track data at 6-hour intervals provided by the Joint Typhoon Warming Center (JTWC; http://www.usno.navy.mil/NOOC/nmfc-ph/RSS/jtwc/best_tracks/wpindex.html).

To analyze the transient fluctuations associated with migratory synoptic-scale disturbances, the meridional wind velocity at periods of 2–8 days in association with synoptic transient eddies at each pressure level is extracted by a Lanczos band-pass filter (Hoskins and Hodges, 2002; Taguchi et al., 2009; Booth et al., 2010; Yao et al., 2016). We use a 5-day moving average of the filtered meridional wind velocity variance (v') as a measure of STEA (Blackmon et al., 1977; Deng and Mak, 2006; Ren et al., 2010). In addition, since STEA can be defined by other forms such as eddy kinetic energy (EKE), we calculated the synoptic transient eddy EKE to validate that the results revealed in this study are independent of the definition of STEA (not shown). The main results presented in this study are based on the analysis of STEA over the North Pacific region (30°–60°N, 130°E–160°W) from October to December during 1979–2019. To identify the influence of TC intensity on STEA strength over the North Pacific, we selected the TCs that move into the region (30°–60°N, 130°E–160°W) after having formed over the tropical WNP and that reach tropical storm intensity (maximum sustained wind speed $\geqslant$17.2 m s^{-1}); there are 144 TCs meeting these conditions, as shown in Fig. 1. TC intensity is represented by the EKE averaged from 1000 hPa to 50 hPa, expressed by $(u'^2 + v'^2)/2$, where u' and v' are the 2–8 days filtered zonal and meridional velocities represented the TC components, respectively. Note that the TC EKE has a high linear correlation with the accumulated cyclone energy (ACE) index proposed by Bell et al. (2000), indicating that this measurement is strongly representative of TC strength. TC EKE is calculated by the mean based on the nearest four grid points of the reanalysis before the cyclone crosses through the western boundary (130°E) or southern boundary (30°N) to move into the target region, according to the JTWC TC best-track dataset. Then, the pentad mean STEA averaged over the North Pacific is calculated beginning from the date the TC enters the target region. Given that the area-weighted STEA on 1 October is already influenced by TCs that may have entered the domain within the previous five days, we perform a detailed investigation of the TC EKE and the area-weighted mean STEA for the selected 144 cases from 26 September to 30 December during 1979–2019. Linear regression and composite analysis methods are used in this study, and the F and Student's t tests are used to show the statistical significance of the regressions and composite analyses, respectively.

3. Results

3.1. *Relationship between TCs and STEA during 1979–2019*

Figure 1 shows the composite distributions of pentad mean STEA after the dates when the selected 144 TCs entered the North Pacific from October to December in the

period 1979–2019. It can be seen that the strongest STEA is located at the upper levels, and it decreases down to the lower levels. The maximum STEA at 300 hPa is located around 45°N, 170°W, with a peak value above 20 m^{-2} s^{-2} (Fig. 1a). The STEA at 500 hPa exhibits a zonal distribution east of (45°N, 150°E) (Fig. 1b), and the maximum intensity of STEA at 850 hPa exhibits a southwest–northeast oriented pattern, with a positive center maximum value of about 8 m^{-2} s^{-2} near 45°N, 165°E over the KOE region (Fig. 1c). It is noteworthy that the spatial distribution of STEA at 850 hPa is apparently different from the spatial distributions at 500 hPa and 300 hPa. The distribution of STEA associated with TCs at 850 hPa is roughly located over the mean path of most of the TCs which take northeastward tracks after recurving and entering the KOE region. We speculate that the STEA in the lower troposphere might

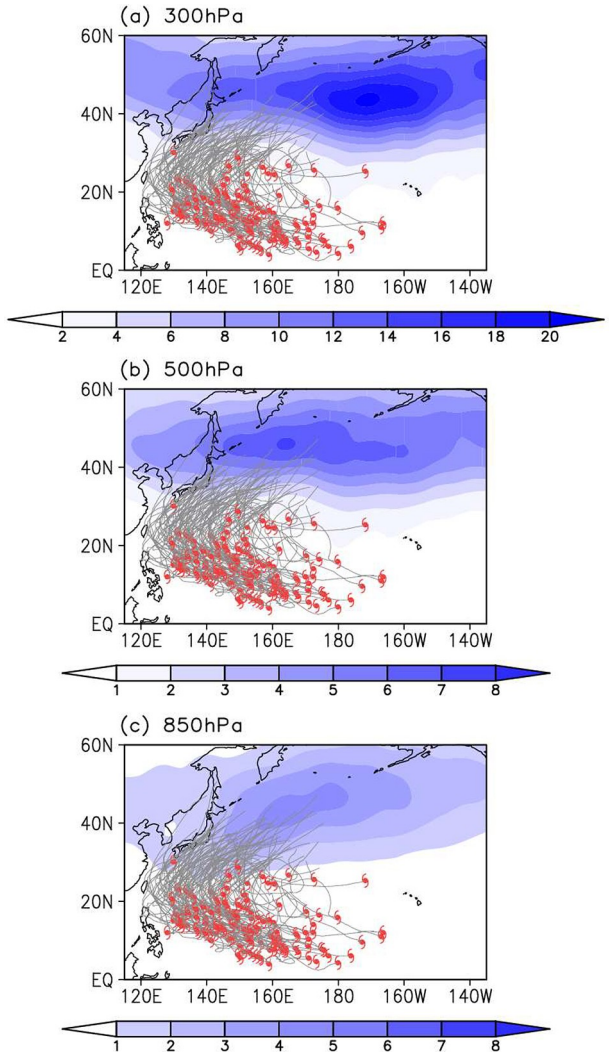

Fig. 1. Composite distributions of pentad mean synoptic-scale transient eddy activity (STEA; shading; m^2 s^{-2}) in the period 1979–2019 at 300 hPa (a), 500 hPa (b), and 850 hPa (c) after the date when the tropical cyclone (TC) entered the North Pacific (30°–60°N, 130°E–160°W) for the selected 144 TC cases. Red TC symbols and gray lines denote genesis locations and tracks of TCs, respectively.

be related to the momentum transfer by the TC vortices. At the mid-to-upper levels, the amplification of eddy perturbations is controlled by a preexisting Rossby wave train that disperses downstream and modifies the large-scale flow patten associated with the TC–extratropical flow interactions (Archambault et al., 2015). Additionally, the spatial patterns of the climatological STEA from October to December are quite similar to those connected with the TCs that enter the KOE region at all levels of the troposphere (not shown).

To explore the relationship between the STEA and TC intensity, Fig. 2 shows the scatter diagram of the TC EKE with the pentad mean STEA for the selected 144 TC cases. On the whole, the positive linear correlation is significant in October and November, but significance is not evident in December due to the small sample size (Figs. 2c, f, and i). A linear relationship of TC EKE with the corresponding STEA intensity can be seen in October and November from the regression polynomial (Figs. 2a, b, d, e, g, and h). STEA intensity is significantly correlated with TC EKE, with a correlation coefficient of 0.39/0.32/0.41 (0.49/0.64/0.68), exceeding the 95% confidence level, at 300 hPa/500 hPa/850 hPa in October (November) (Table 1). Due to the very small number of TC cases in December, there is almost no linear relationship between TC EKE and STEA. In general, TC intensity is highly indicative of the subsequent STEA, with a correlation coefficient of 0.37/0.33/0.45, exceeding the 99% confidence level, at 300 hPa/500 hPa/850 hPa from October to December for the period 1979–2019 (Table 1). Meanwhile, STEA reaches its most significant correlation with TC EKE in the lower troposphere from October to November. This is possible because TC activity, accompanied by abundant kinetic energy, is transported into the target region at the lower levels, favoring more transient eddy development over the North Pacific and thus combining the lower-level STEA with TC EKE. Most STEA cases in November are located more closely around the linear regression polynomial, indicating that the intensity of STEA associated with TC activity in November is stronger than that in October and December. This is partially attributed to the peak strength of STEA over the North Pacific occurring in November, as well as simultaneous intense TCs entering into this region when the climatological STEA values are already high (not shown).

To further examine the influence of TC activity on the spatial variation of STEA intensity, results of the regressions performed on the TC EKE series of the 144 TC cases for pentad mean STEA in the troposphere are shown in Fig. 3. It can be seen that although the linear contribution of TC activity to STEA exhibits a spatial discrepancy between different atmospheric levels, the positive impacts of TCs on STEA are consistent throughout the entire troposphere, and this is highlighted by the robust positive regression coefficients. As shown in Fig. 3a (3b), the most significant regression coefficients in association with strong STEA are characterized by a tripolar pattern, with three maximum centers from west to east, located around (45°N, 140°E), (45°N,

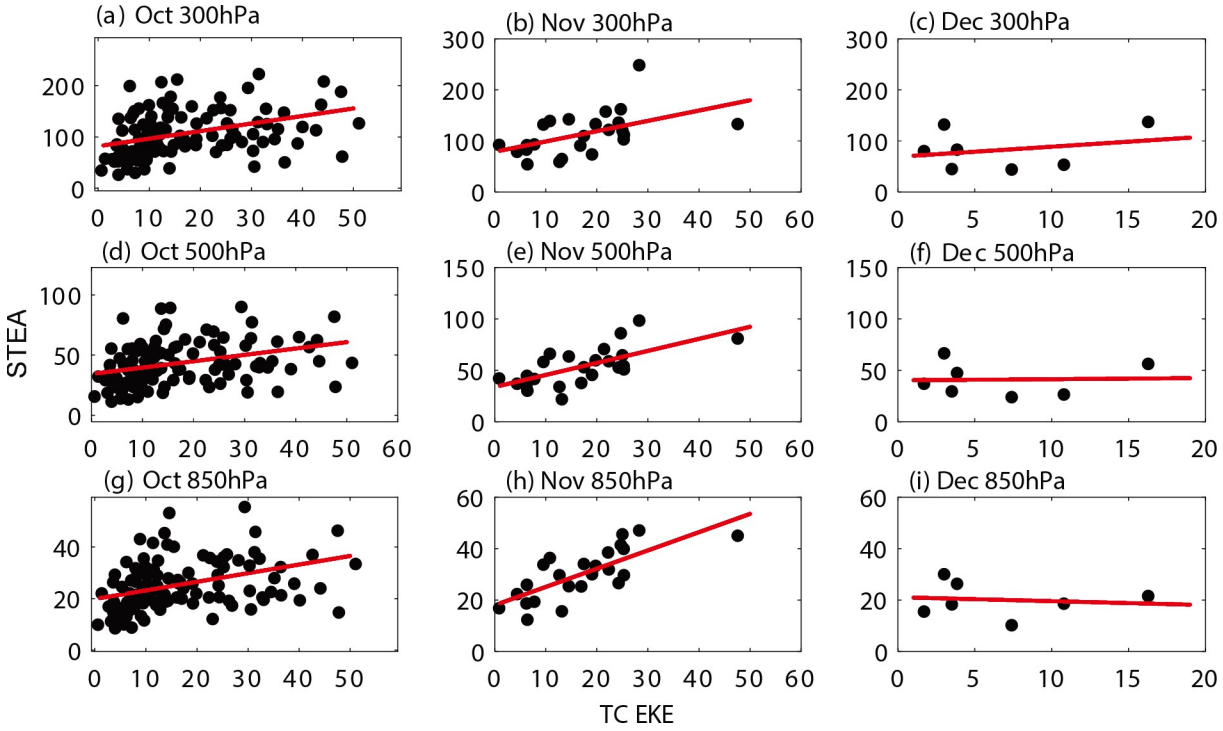

Fig. 2. Scatter diagrams of TC eddy kinetic energy (EKE; $m^2 s^{-2}$) with pentad mean STEA ($m^2 s^{-2}$) at 300 hPa [(a), (b), (c)], 500 hPa [(d), (e), (f)], and 850 hPa [(g), (h), (i)] for the selected 113 TC cases in October (left), 24 TC cases in November (middle), and 7 TC cases in December (right). Red lines are linear regression curves, and the correlation coefficients between the TC EKE and STEA are listed in Table 1.

Table 1. Correlation coefficients matrix between the TC EKE and corresponding STEA from October to December in the period 1979–2019.

	October	November	December	October to December
300 hPa	0.39**	0.49*	0.23	0.37**
500 hPa	0.32**	0.64**	–0.01	0.33**
850 hPa	0.41**	0.68**	–0.10	0.45**

* Significant at the 95% confidence level.
** Significant at the 99% confidence level.

175°E), and (45°N, 170°W) [(42°N, 160°E), (40°N, 170°E), and (40°N, 170°W)] at 300 hPa (500 hPa), respectively. Yet, the evident positive regression relationship between the TC EKE and STEA at 850 hPa is largely concentrated west of 165°E, exhibiting a northeast–southwest-oriented pattern from south of Japan to the northwestern WNP. These results suggest that TC activity can exert great influences on a broad area at the mid-to-upper levels, migrating eastward to the Northeast Pacific. Meanwhile, in the lower troposphere, the impact of TCs on STEA is primarily localized over the KOE region. Additionally, based on the distribution of standard regression coefficients, the significant positive contribution of TCs to STEA at the upper levels is located over the central North Pacific (Fig. 3a), which is more extensive than the contribution at the mid-to-lower levels (Figs. 3b and c). The results of monthly regression show that the contribution of TCs to STEA in October is largest in late autumn and early winter, and the contribution of TCs in November and December is less based on the significant region (Figs. 3g–3l), as there are fewer TC samples in these two months.

3.2. *Interannual variation of TC contribution to STEA*

We also examine the interannual change of the relationship between the TC EKE and STEA by calculating the interannual means of TC EKE and pentad mean STEA cases from 1979 to 2019. Figure 4a shows the scatter diagrams of annual-averaged TC EKE and STEA for 41 years at different atmospheric levels during 1979–2019, respectively. It is noted that the TC EKE index is significantly correlated with the subsequent STEA at 300 hPa/500 hPa/850 hPa/all level over the North Pacific at the interannual time scale, with a correlation coefficient of 0.52/0.44/0.49/0.47, exceeding the 99% confidence level. The strongest correlation on the interannual time scale is located in the upper troposphere, which reflects a long time-scale variability and is different from the results shown in Table 1. Based on the slope of the linear regression curve, STEA in the upper troposphere (300 hPa) exhibits a more significant linear growth relation-

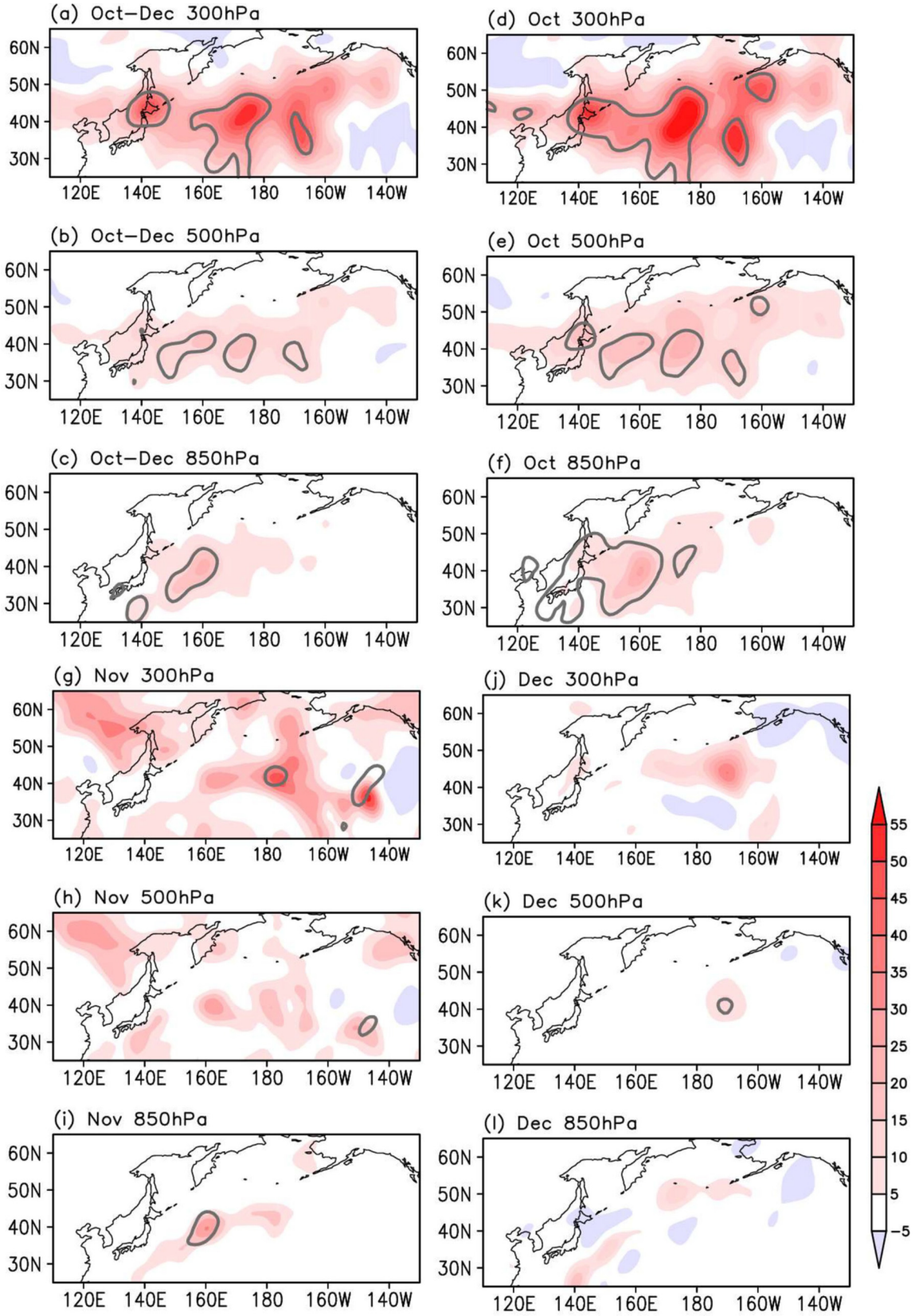

Fig. 3. Simultaneous regression upon normalized TC EKE for pentad mean STEA (shading; $m^2\ s^{-2}$) at 300 hPa [(a), (d), (g), (j)], 500 hPa [(b), (e), (h), (k)], and 850 hPa [(c), (f), (i), (l)] for the selected 144 TC cases during October–December (left), 113 TC cases in October (left-center), 24 TC cases in November (right-center), and 7 TC cases in December (right). Anomalies enclosed by gray contours denote the coefficients are significant above the 95% confidence level by the *F* test.

ship with TC EKE than that in the mid-to-lower levels during the period after cyclones enter the KOE region (Fig. 4a). This suggests that the impact of TCs on STEA has an effect that gradually increases with height, which is closely related to the interaction between TCs and the westerly jet in the upper troposphere (Archambault et al., 2015; Chen et al., 2017). Moreover, the results of simultaneous regression exhibit a strong spatial variation of STEA at 300 hPa connected with TC activity broadly located over the western and central North Pacific (35°–45°N, west of around 180°; Fig. 4b), which is similar to the significant regions at 500 hPa and 850 hPa (Figs. 4c and 4d). This agreement throughout the entire troposphere suggests a consistent feature at the interannual time scale of TC influence on STEA changes over the North Pacific. This interannual influence is probably connected with the development of downstream wave packets associated with the TCs in the extratropical baroclinic storm-track region in a climatological sense (Archambault et al., 2015; Keller et al., 2019).

Figures 5a, e, and f show the temporal strength distributions of the pentad mean STEA overlapped with the TCs when they enter the KOE region from October to December in the period 1979–2019. During the annual cycle, there is a minimum in the strength of the climatological STEA over the North Pacific in midwinter (Nakamura, 1992). Before the midwinter suppression, STEA reaches its strongest intensity during autumn to early winter (October through December). In particular, the strongest STEA is located at the upper levels and decreases with reduced height. The total STEA over the North Pacific from October to December displays interannual (Figs. 5b and f) and interdecadal variations (Fig. 5j). Figures 5c, g, and k show the interannual series of STEA associated with the entered TCs at 300 hPa, 500 hPa, and 850 hPa, respectively. There is a high linear correlation between their changes, indicating that the effect of TCs on STEA is consistent throughout the whole troposphere on the interannual time scale. In order to further study the quantitative contribution of TCs to STEA, the ratios of STEA associated with the entered TCs to the total STEA at the different levels are calculated and shown in Figs. 5d, h, and l. From the October–December climatic average, the ratio in the North Pacific is 4.24%/4.48%/6.18% at 300 hPa/500 hPa/850 hPa. That is, the contribution of TCs to STEA in late autumn and early winter reaches about 4%–6%. In addition, the contribution of TCs to the STEA in autumn and early winter experienced an interdecadal

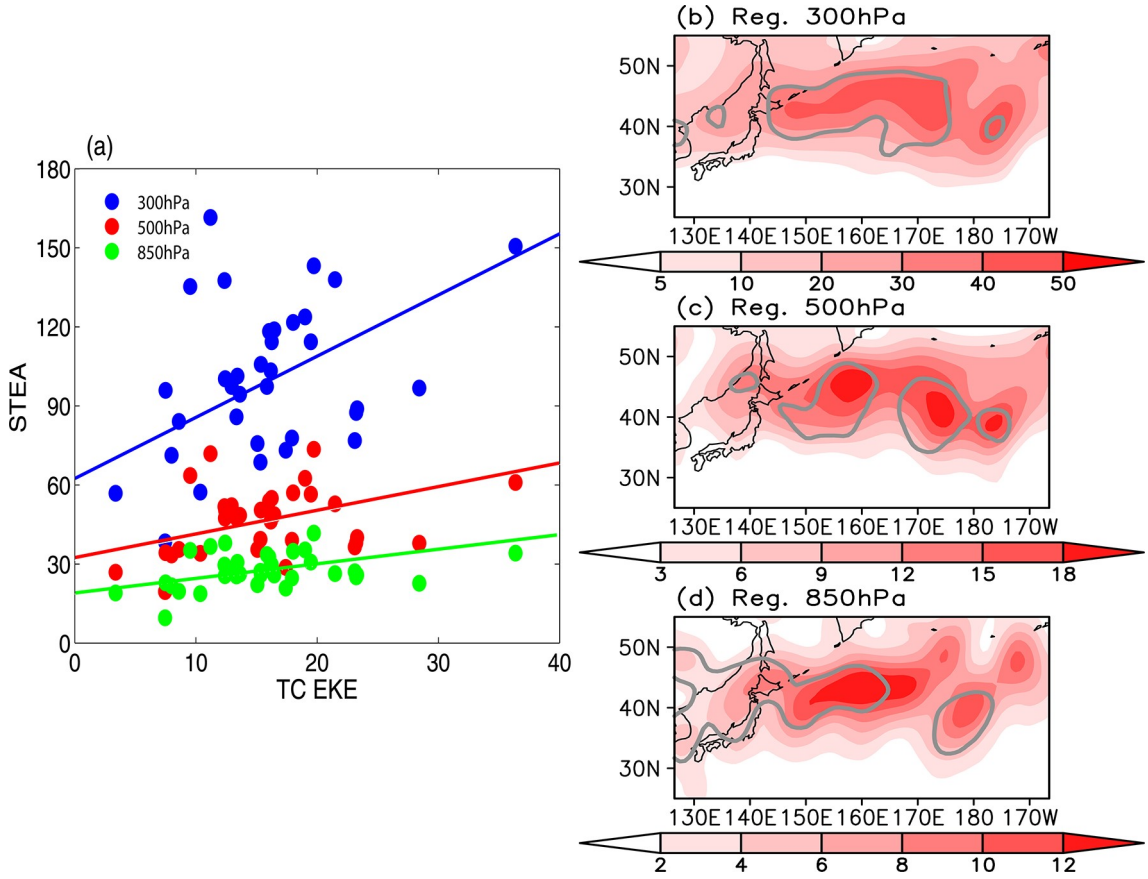

Fig. 4. (a) Scatter diagrams of TC EKE (m^2 s^{-2}) with pentad mean STEA (m^2 s^{-2}) from October to December for 41 years in the period 1979–2019. Lines are linear regression curves at the different levels. Simultaneous regression upon annual-mean normalized TC EKE for pentad mean STEA (shading; m^2 s^{-2}) at 300 hPa (b), 500 hPa (c), and 850 hPa (d) from 1979 to 2019. Anomalies enclosed by gray contours in (b)–(d) denote the coefficients are significant above the 95% confidence level by the *F* test.

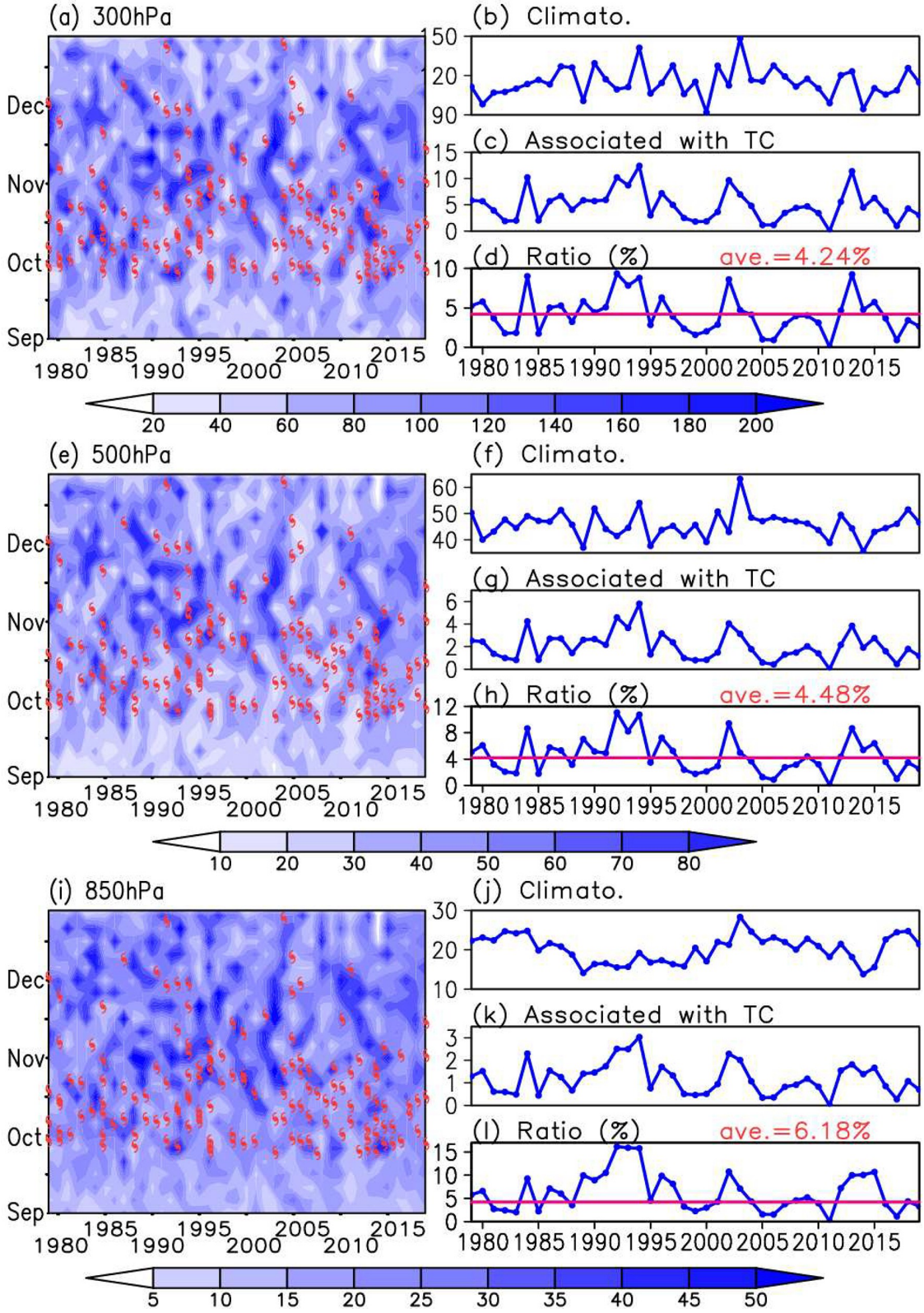

Fig. 5. Distributions of pentad mean STEA intensity (shading; $m^2\ s^{-2}$) averaged over the North Pacific (30°–60°N, 130°E–160°W) at 300 hPa (a), 500 hPa (e), and 850 hPa (i) overlapped with the red TC symbols when a TC entered the Kuroshio/Oyashio Extensions. Interannual variations of the total STEA [$m^2\ s^{-2}$; (b), (f), (j)], the STEA associated with the entered TCs [$m^2\ s^{-2}$; (c), (g), (k)], and the ratio of STEA associated with the entered TCs to the total STEA [%; (d), (h), (l)] at 300 hPa (upper-right), 500 hPa (middle-right), and 850 hPa (lower-right) from October to December. The red lines and percentages denote the averaged ratio of STEA associated with the entered TCs to the total STEA in the period 1979–2019.

change in the early 2000s, which can be detected at each level of the troposphere. Compared to the higher ratios before the 2000s, there is a marked decrease from the early 2000s through the early 2010s (Figs. 5d, h, and l). In order to clarify the spatial characteristics of the interannual variation of TC influence on STEA, the anomalies of STEA in the composited TC high-impact and low-impact years in the period 1979–2019 are presented in Fig. 6. In general, the anomaly distribution of STEA presents the opposite phase in the TC high-impact and low-impact years, and the positive anomalies of STEA have a wider range during the high-impact years (Figs. 6a, c, and e). In addition, the significant area affected by the anomaly is different between east and west and between upper levels and lower levels.

In this study, to establish the quantitative relationship between TCs and STEA, we calculate the TC EKE before a cyclone crosses through the boundaries (130°E or 30°N) of the North Pacific region, and we calculate the pentad mean STEA beginning on the date when the selected TC enters the KOE zone. This is a traditional method to parameterize the transient eddy activity in synoptic disturbances, including TCs (Ren et al., 2010; Ha et al., 2013). In fact, considering the definition of STEA, which is calculated by the variance of meridional velocity averaged for a certain period of several days, we also detect the lagging relationship between TC EKE and STEA defined by the different period-means. Figure 7 shows the correlation coefficients between TC EKE and STEA calculated by the n day-mean; please note that the results presented in this paper correspond to the condition of $n = 5$ (pentad mean). It can be seen that STEA defined by the mean variance within a period of 12 days-mean/10 days-mean/13 days-mean all have significant linear relationships with the TC EKE at 300 hPa/500 hPa/850 hPa, which can exceed the 95% confidence level (Fig. 7). This suggests that from a climatology perspective, the impact of TC activity on STEA over the North Pacific can last as long as two pentads after a TC enters the mid-latitudinal region. Meanwhile, the effective temporal lengths of TC influence on the STEA at the lower and upper levels are slightly longer than that at the midlevel (12 days/11 days vs. 9 days). In addition, we also calculated the relationship between TCs and STEA defined by the synoptic transient eddy EKE at different levels, and similar conclusions can be drawn (not shown). This suggests that the relationship revealed in this study between TC activity and the strength of STEA over the North Pacific is independent of the definition of STEA.

4. Discussions

Observational results show the significant positive correlation on the interannual time scale between WNP TC activity and STEA strength over the KOE region during October to December in the period 1979–2019. TCs have been known to play a potential role in the exchange and balance of energy and material between the tropics and higher latitudinal regions. On the other hand, it is also known that the El Niño-Southern Oscillation (ENSO) is one of the most important factors that modulate the interannual variability of TC activity over the Pacific Ocean (Chan, 2000; Chia and Ropelewski, 2002; Wang and Chan, 2002; Sobel and Camargo, 2005). During El Niño years, most TCs form over the southeastern WNP and experience stronger intensities, longer life spans, and tracks that recurve around 130°E and then move northeastward into the KOE region. In particular, TCs that form in the southeastern WNP intensify more easily due to having more time over its warm waters, and thus, they have the opportunity to transport massive amounts of momentum and heat to the atmosphere over the midlatitudes. In contrast, the opposite situation occurs during La Niña years, and more TCs that form over the western part of the WNP take westward tracks and make landfall over the Philippines and southern China (Ha and Zhong, 2014). Thus, fewer cyclones can move into the midlatitudes. This indicates that the strength of STEA from October to December may be enhanced (weakened) by more (less) frequent intense TCs during El Niño (La Niña) events. Meanwhile, previous studies have revealed that ENSO has a significant influence on the maintenance of STEA over the North Pacific (Straus and Shukla, 1997; Zhu and Sun, 1999; Eichler and Higgins, 2006; Wang et al., 2013). During El Niño (La Niña) events, the strength of STEA increases (decreases), and its position extends (withdraws) more southward (northward) in response to the interannual change of eddy heat and momentum fluxes. Note that the year-to-year change of STEA during October to December is concurrently correlated to the Niño-3.4 index for the period 1979–2019 (the correlation coefficient is 0.29, exceeding the 90% confidence level). It implies that the direct modulation of ENSO on STEA is consistent with the effect of TC contributions to STEA to a certain extent. This study demonstrates that TC activity can provide a source of climatological predictability that extends ENSO impacts to midlatitudes over the North Pacific and motivates an area of research around how changes in TCs may influence interannual and future changes of STEA. Whether TCs can be considered as a new pathway to understand the multi-variability of STEA under the background of global change remains an open problem. In a future study, detailed mechanisms for the impact of TCs on the multi-scale changes of STEA over the North Pacific will be analyzed quantitatively by the combination of observational data and numerical experiments.

5. Concluding remarks

The results of this study show that WNP TCs entering the mid-latitudinal North Pacific provide significant positive contributions to the pentad mean strength of STEA. The linear impact of TC activity on the pentad mean STEA in the lower troposphere is primarily concentrated over the KOE region and extends eastward to the northeastern North Pacific at the mid-to-upper levels. The TC EKE is highly

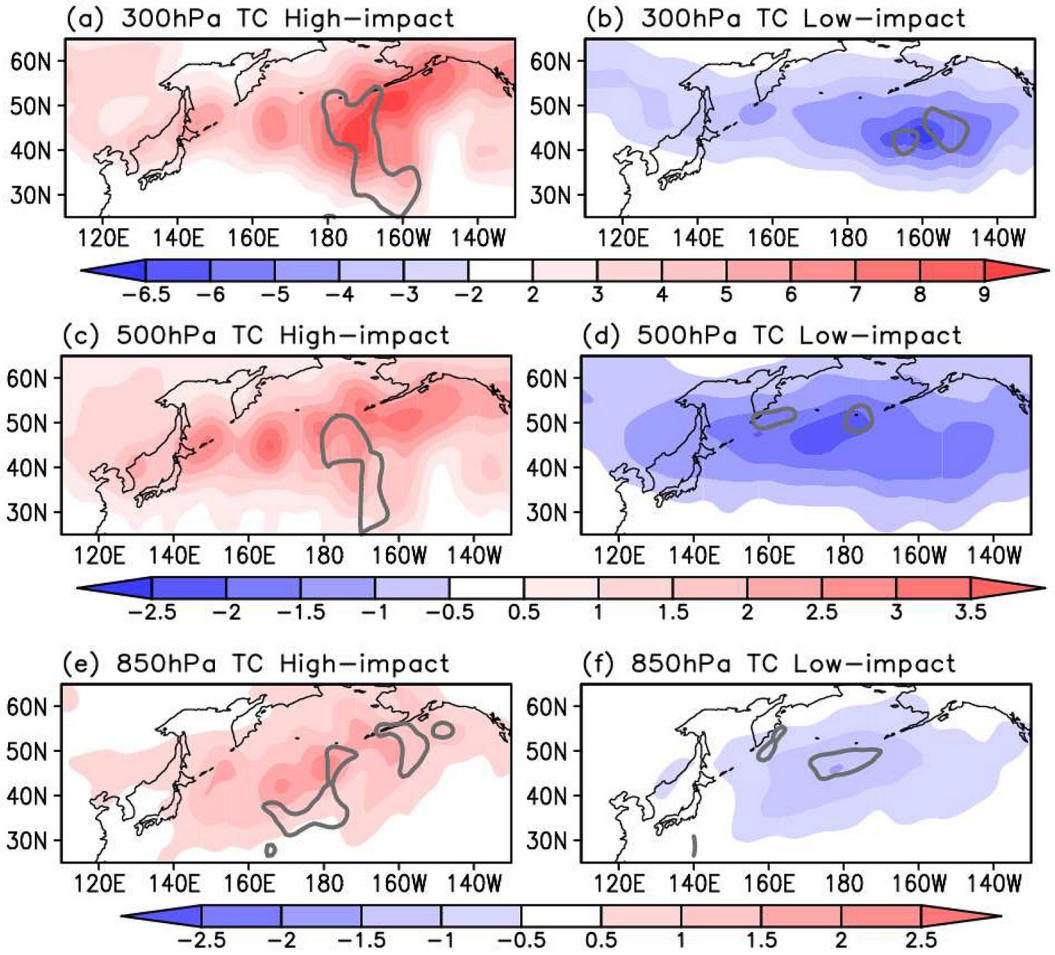

Fig. 6. Anomalies of pentad mean STEA (shading; $m^2\ s^{-2}$) in the composited TC high-impact years [(a), (c), (e)] and low-impact years [(b), (d), (f)] in the period 1979–2019 at 300 hPa (top), 500 hPa (middle), and 850 hPa (bottom) based on the thresholds with one standard deviation of normalized ratios of the STEA associated with TCs to the total STEA in Figs. 5d, 5h, and 5l. The high-impact (low-impact) years are 1992, 1993, 1994, 1996, 2002, and 2013 (1982, 1983, 1985, 1991, 2005, 2006, 2011, and 2017). Differences enclosed by solid contours denote that the anomalies are significant above the 95% confidence level by the two tailed Student's *t* test.

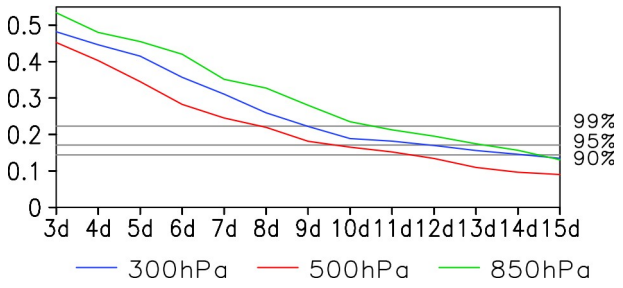

Fig. 7. TC EKE correlation coefficient with *n* day-mean STEA after the date when TCs enter the North Pacific (30°–60°N, 130°E–160°W) at 300 hPa, 500 hPa, and 850 hPa for the 144 TC cases.

indicative of the subsequent STEA with a correlation coefficient of 0.37/0.33/0.45, exceeding the 99% confidence level, at 300 hPa/500 hPa/850 hPa for the period 1979–2019. The spatial distribution of TC impacts on STEA displays a latitudinal tripolar pattern at 300 hPa and 500 hPa but exhibits a northeast–southwest-oriented pattern east of Japan at 850 hPa. The strength of STEA in the upper troposphere presents a more significant linear growth with TC EKE than that at the mid-to-lower levels after cyclones enter the KOE region, suggesting that the impact of TCs on STEA has an effect that gradually increases with height. The ratios of STEA associated with the entered TCs to the total STEA in North Pacific reaches 4.24%/4.48%/6.18% at 300 hPa/500 hPa/850 hPa. On the whole, the contribution of TCs to STEA in late autumn and early winter is about 4%–6%. In addition, the contribution of TCs to the STEA in autumn and early winter experiences an interdecadal decrease from the early 2000s through the early 2010s. The significant relationship between TC intensity and STEA strength indicates that the synoptic-scale eddy disturbances over the North Pacific may have partial origins in WNP TCs. Previous studies have revealed that the frequency and amplitude of disturbances entering the North Pacific from Siberia via mid-to-high-latitudinal Asia can control the

strength of STEA over the North Pacific (Orlanski, 2005; Zurita-Gotor and Chang, 2005; Penny et al., 2010; Chang and Guo, 2012). Additionally, the amplification of a preexisting Rossby wave train closely related to the recurving TCs over the WNP can modify the large-scale flow pattern over the mid-latitudinal North Pacific and North America (Anwender et al., 2008; Harr et al., 2008; Harr and Dea, 2009; Archambault et al., 2015). This implies that WNP TC activity can exert influence through the teleconnection induced by TC–extratropical flow interactions to modulate STEA strength (Kawamura and Ogasawara, 2006; Grams and Archambault, 2016). In the current study, we present a climatological perspective on STEA response to WNP TC intensity during boreal autumn and early winter, and we hope the observational results will help explain the influence and contribution of TCs to the synoptic-scale system activity in the midlatitudes.

Acknowledgements. All authors contributed equally to this study and share first authorship. This work is sponsored jointly by the National Key Basic Research Program (2018YFC1505905), National Natural Science Foundation of China (Grant Nos. 41975090, 41922033, 41675077, and 42005025), Scientific Research Program of National University of Defense Technology (18/19-QNCXJ), the Jiangsu Collaborative Innovation Center for Climate Change in Nanjing University, and the Jiangsu Collaborative Innovation Center on Forecast and Evaluation of Meteorological Disasters.

REFERENCES

Anwender, D., P. A. Harr, and S. C. Jones, 2008: Predictability associated with the downstream impacts of the extratropical transition of tropical cyclones: Case studies. *Mon. Wea. Rev.*, **136**, 3226–3247, https://doi.org/10.1175/2008MWR2249.1.

Archambault, H. M., L. F. Bosart, D. Keyser, and J. M. Cordeira, 2013: A climatological analysis of the extratropical flow response to recurving Western North Pacific tropical cyclones. *Mon. Wea. Rev.*, **141**, 2325–2346, https://doi.org/10.1175/MWR-D-12-00257.1.

Archambault, H. M., D. Keyser, L. F. Bosart, C. A. Davis, and J. M. Cordeira, 2015: A composite perspective of the extratropical flow response to recurving Western North Pacific tropical cyclones. *Mon. Wea. Rev.*, **143**, 1122–1141, https://doi.org/10.1175/MWR-D-14-00270.1.

Bell, G. D., and Coauthors, 2000: Climate assessment for 1999. *Bull. Amer. Meteor. Soc.*, **81**, S1–S50, https://doi.org/10.1175/1520-0477(2000)81[s1:CAF]2.0.CO;2.

Blackmon, M. L., J. M. Wallace, N.-C. Lau, and S. L. Mullen, 1977: An observational study of the Northern Hemisphere wintertime circulation. *J. Atmos. Sci.*, **34**, 1040–1053, https://doi.org/10.1175/1520-0469(1977)034<1040:AOSOTN>2.0.CO;2.

Booth, J. F., L. A. Thompson, J. Patoux, K. A. Kelly, and S. Dickinson, 2010: The signature of the midlatitude tropospheric storm tracks in the surface winds. *J. Climate*, **23**, 1160–1174, https://doi.org/10.1175/2009JCLI3064.1.

Chan, J. C. L., 2000: Tropical cyclone activity over the western North Pacific associated with El Niño and La Niña events. *J. Climate*, **13**, 2960–2972, https://doi.org/10.1175/1520-0442(2000)013<2960:TCAOTW>2.0.CO;2.

Chang, E. K. M., 2001: GCM and observational diagnoses of the seasonal and interannual variations of the Pacific storm track during the cool season. *J. Atmos. Sci.*, **58**, 1784–1800, https://doi.org/10.1175/1520-0469(2001)058<1784:GAODOT>2.0.CO;2.

Chang, E. K. M., and S. Song, 2006: The seasonal cycles in the distribution of precipitation around cyclones in the western North Pacific and Atlantic. *J. Atmos. Sci.*, **63**, 815–839, https://doi.org/10.1175/JAS3661.1.

Chang, E. K. M., and Y. J. Guo, 2007: Dynamics of the stationary anomalies associated with the interannual variability of the midwinter Pacific storm track—The roles of tropical heating and remote eddy forcing. *J. Atmos. Sci.*, **64**, 2442–2461, https://doi.org/10.1175/JAS3986.1.

Chang, E. K. M., and Y. J. Guo, 2012: Is Pacific storm-track activity correlated with the strength of upstream wave seeding. *J. Climate*, **25**, 5768–5776, https://doi.org/10.1175/JCLI-D-11-00555.1.

Chang, E. K. M., S. Lee, and K. L. Swanson, 2002: Storm track dynamics. *J. Climate*, **15**, 2163–2183, https://doi.org/10.1175/1520-0442(2002)015<02163:STD>2.0.CO;2.

Chen, X., Z. Zhong, and W. Lu, 2017: Association of the poleward shift of East Asian subtropical upper-level jet with frequent tropical cyclone activities over the western North Pacific in summer. *J. Climate*, **30**, 5597–5603, https://doi.org/10.1175/JCLI-D-16-0334.1.

Chia, H. H., and C. F. Ropelewski, 2002: The interannual variability in the genesis location of tropical cyclones in the northwest Pacific. *J. Climate*, **15**, 2934–2944, https://doi.org/10.1175/1520-0442(2002)015<2934:TIVITG>2.0.CO;2.

Cordeira, J. M., F. M. Ralph, and B. J. Moore, 2013: The development and evolution of two atmospheric rivers in proximity to Western North Pacific tropical cyclones in October 2010. *Mon. Wea. Rev.*, **141**, 4234–4255, https://doi.org/10.1175/MWR-D-13-00019.1.

Deng. Y., and M. Mak, 2006: Nature of the differences in the intraseasonal variability of the Pacific and Atlantic storm tracks: A diagnostic study. *J. Atmos. Sci.*, **63**, 2602–2615, https://doi.org/10.1175/JAS3749.1.

Eichler, T., and W. Higgins, 2006: Climatology and ENSO-related variability of North American extratropical cyclone activity. *J. Climate*, **19**, 2076–2093, https://doi.org/10.1175/JCLI3725.1.

Grams, C. M., and H. M. Archambault, 2016: The key role of diabatic outflow in amplifying the midlatitude flow: A representative case study of weather systems surrounding western North Pacific extratropical transition. *Mon. Wea. Rev.*, **144**, 3847–3869, https://doi.org/10.1175/MWR-D-15-0419.1.

Ha, Y., and Z. Zhong, 2014: Features of tropical cyclone landfalls over East Asia corresponding to three types of Pacific warming decaying phase. *Chinese Science Bulletin*, **59**, 4130–4136, https://doi.org/10.1007/s11434-014-0582-1.

Ha, Y., Z. Zhong, Y. M. Zhu, and Y. J. Hu, 2013: Contributions of barotropic energy conversion to northwest Pacific tropical cyclone activity during ENSO. *Mon. Wea. Rev.*, **141**, 1337–1346, https://doi.org/10.1175/MWR-D-12-00084.1.

Harr, P. A., and J. M. Dea, 2009: Downstream development associated with the extratropical transition of tropical cyclones over the western North Pacific. *Mon. Wea. Rev.*, **137**,

1295–1319, https://doi.org/10.1175/2008MWR2558.1.

Harr, P. A., R. L. Elsberry, and T. F. Hogan, 2000: Extratropical transition of tropical cyclones over the western North Pacific. Part II: The impact of midlatitude circulation characteristics. *Mon. Wea. Rev.*, **128**, 2634–2653, https://doi.org/10.1175/1520-0493(2000)128<2634:ETOTCO>2.0.CO;2.

Harr, P. A., D. Anwender, and S. C. Jones, 2008: Predictability associated with the downstream impacts of the extratropical transition of tropical cyclones: Methodology and a case study of Typhoon Nabi (2005). *Mon. Wea. Rev.*, **136**, 3205–3225, https://doi.org/10.1175/2008MWR2248.1.

Hoskins, B. J., and K. I. Hodges, 2002: New perspectives on the Northern Hemisphere winter storm tracks. *J. Atmos. Sci.*, **59**, 1041–1061, https://doi.org/10.1175/1520-0469(2002)059<1041:NPOTNH>2.0.CO;2.

Kalnay, E., and Coauthors, 1996: The NCEP/NCAR 40-year reanalysis project. *Bull. Amer. Meteor. Soc.*, **77**, 437–472, https://doi.org/10.1175/1520-0477(1996)077<0437:TNYRP>2.0.CO;2.

Kawamura, R., and T. Ogasawara, 2006: On the role of typhoons in generating PJ teleconnection patterns over the western North Pacific in late summer. *SOLA*, **2**, 37–40, https://doi.org/10.2151/sola.2006-010.

Keller, J. H., 2017: Amplification of the downstream wave train during extratropical transition: Sensitivity studies. *Mon. Wea. Rev.*, **145**, 1529–1548, https://doi.org/10.1175/MWR-D-16-0193.1.

Keller, J. H., and Coauthors, 2019: The extratropical transition of tropical cyclones. Part II: Interaction with the midlatitude flow, downstream impacts, and implications for predictability. *Mon. Wea. Rev.*, **147**, 1077–1106, https://doi.org/10.1175/MWR-D-17-0329.1.

Nakamura, H., 1992: Midwinter suppression of baroclinic wave activity in the Pacific. *J. Atmos. Sci.*, **49**, 1629–1642, https://doi.org/10.1175/1520-0469(1992)049<1629:MSOBWA>2.0.CO;2.

Nakamura, H., and T. Sampe, 2002: Trapping of synoptic-scale disturbances into the North-Pacific subtropical jet core in midwinter. *Geophys. Res. Lett.*, **29**, 8-1–8-4, https://doi.org/10.1029/2002GL015535.

Orlanski, I., 2005: A new look at the Pacific storm track variability: Sensitivity to tropical SSTs and to upstream seeding. *J. Atmos. Sci.*, **62**, 1367–1390, https://doi.org/10.1175/JAS3428.1.

Penny, S., G. H. Roe, and D. S. Battisti, 2010: The source of the midwinter suppression in storminess over the North Pacific. *J. Climate*, **23**, 634–648, https://doi.org/10.1175/2009JCLI2904.1.

Ren, X. J., X. Q. Yang, and C. J. Chu, 2010: Seasonal variations of the synoptic-scale transient eddy activity and polar front jet over East Asia. *J. Climate*, **23**, 3222–3233, https://doi.org/10.1175/2009JCLI3225.1.

Ren, X. J., X. Q. Yang, T. J. Zhou, and J. B. Fang, 2011: Diagnostic comparison of wintertime East Asian subtropical jet and polar-front jet: Large-scale characteristics and transient eddy activities. *Acta Meteorologica Sinica*, **25**, 21–33, https://doi.org/10.1007/s13351-011-0002-2.

Sobel, A. H., and S. J. Camargo, 2005: Influence of western North Pacific tropical cyclones on their large-scale environment. *J. Atmos. Sci.*, **62**, 3396–3407, https://doi.org/10.1175/JAS3539.1.

Straus, D. M., and J. Shukla, 1997: Variations of midlatitude transient dynamics associated with ENSO. *J. Atmos. Sci.*, **54**, 777–790, https://doi.org/10.1175/1520-0469(1997)054<0777:VOMTDA>2.0.CO;2.

Taguchi, B., H. Nakamura, M. Nonaka, and S.-P. Xie, 2009: Influences of the Kuroshio/Oyashio Extensions on air–sea heat exchanges and storm-track activity as revealed in regional atmospheric model simulations for the 2003/04 cold season. *J. Climate*, **22**, 6536–6560, https://doi.org/10.1175/2009JCLI2910.1.

Wang, B., and J. C. L. Chan, 2002: How strong ENSO events affect tropical storm activity over the western North Pacific. *J. Climate*, **15**, 1643–1658, https://doi.org/10.1175/1520-0442(2002)015<1643:HSEEAT>2.0.CO;2.

Wang, B., B. Q. Xiang, and J.-Y. Lee, 2013: Subtropical high predictability establishes a promising way for monsoon and tropical storm predictions. *Proceedings of the National Academy of Sciences of the United States of America*, **110**, 2718–2722, https://doi.org/10.1073/pnas.1214626110.

Xiao, C. L., and Y. C. Zhang, 2015: Projected changes of wintertime synoptic-scale transient eddy activities in the East Asian eddy-driven jet from CMIP5 experiments. *Geophys. Res. Lett.*, **42**, 6008–6013, https://doi.org/10.1002/2015GL064641.

Yao, Y., Z. Zhong, and X.-Q. Yang, 2016: Numerical experiments of the storm track sensitivity to oceanic frontal strength within the Kuroshio/Oyashio Extensions. *J. Geophys. Res.*, **121**, 2888–2900, https://doi.org/10.1002/2015JD024381.

Zhao, H. K., and C. Z. Wang, 2016: Interdecadal modulation on the relationship between ENSO and typhoon activity during the late season in the western North Pacific. *Climate Dyn.*, **47**, 315–328, https://doi.org/10.1007/s00382-015-2837-1.

Zhu, W. J., and Z. B. Sun, 1999: Influence of ENSO event on the maintenance of Pacific storm track in the northern winter. *Adv. Atmos. Sci.*, **16**, 630–640, https://doi.org/10.1007/s00376-999-0037-9.

Zurita-Gotor, P., and E. K. M. Chang, 2005: The impact of zonal propagation and seeding on the eddy–mean flow equilibrium of a zonally varying two-layer model. *J. Atmos. Sci.*, **62**, 2261–2273, https://doi.org/10.1175/JAS3473.1.